Efficient Semi-automatic Segmentation for Creating Patient Specific Models for Virtual Environments

Y. Song, A. J. Bulpitt and K. Brodlie

School of Computing, University of Leeds, UK
{yisong, andyb, kwb}@comp.leeds.ac.uk

Abstract. There is an increasing demand for the development of virtual environments for training in vascular interventional radiological procedures. This requires fast and precise segmentation of varied abdominal structures from a wide range of image modalities. This paper presents an efficient semi-automatic segmentation system which combines image processing techniques and mathematical morphology operations to obtain an initial segmentation close to the target structure shape. This initial segmentation is then embedded into a level set function to obtain a refined segmentation result. Minimal intervention is required in comparison to other level set based approaches. The approach also dramatically decreases processing time and reduces the risks of leaking at weak boundaries, without compromising the accuracy of the segmentation.

1 Introduction

Our work is part of the CRaIVE[1] project to develop a physics based Virtual Environment (VE) for training in vascular interventional radiological procedures. It aims to provide an alternative to apprenticeship training using physical and animal models where not only are the traditional physical models expensive, but their fixed anatomy also constrains the training achievements where a wide range of pathology is required to be presented to trainees.

Creating virtual humans for this task requires major abdominal structures to be segmented with particular interest in those cases where typical symptoms are presented. Currently, our data are collected from various hospitals and research institutes in order to cover a large variety of cases. Consequently, the resource images to be segmented vary greatly in quality, size and resolution and the presented abdominal structures are typically significantly different from those found in healthy cases.

A myriad of different segmentation methods have been proposed and implemented in recent years. See [SLR*02] [KQ04] [CC07] for recent reviews. Model-driven, knowledge based image analysis is one of the techniques often used; this aims to describe and capture a priori information regarding the shape, size and position of each structure. Normally deformable models [GHF98], statistical shape models [HMW07] and probabilistic atlases [PBM03] are employed. The limitation of these approaches is the generation of a suitable template model which is able to capture both natural variations and deformations caused by pathology. As our system needs to handle various abnormalities, sometimes with extreme shape deformation, current model-driven approaches are not well suited to our application.

In addition, the varied image modalities further limit the applications of previous segmentation techniques. For example, approaches based on the region growing technique [PT01] or mathematical morphology operations [YCN*00] such as DTT (Differential tip-hats) and conditional dilation etc., can provide good results on contrast-enhanced images. However since these techniques are based on the image intensity similarity, when adjacent neighbouring tissues have similar intensity to the target structure, the region growing approach is easily over segmented, while mathematical morphology operations could fail to divide the adjoining tissues completely.

Approaches based on the level set method [Set99] [CKS97] have also been used successfully for medical image segmentation. However, the problem of "leaks" on the boundary is still open to research. Pan and Dawant [PD01] propose to progressively slow down the speed as the front passes over boundary points. They also added a priori anatomical information to the accumulative speed function. Other drawbacks include its sensitivity to positioning seeds in the volume data and the non-trivial work of setting parameters according to the image modalities and object structures [WBM*01]. Tools [MBW*05] [WTH*98] have been developed to allow interactive editing of level set models.

In this paper, we are interested in developing a general solution to recovering abnormal structures in

[1] Collaborators in Radiological Interventional Virtual Environments, http://www.craive.org.uk

real time with minimal user interaction. In contrast to previous work focusing on either specified image type, (e.g. CT or MR image [SLR*02]) or specified structures (e.g. liver or vascular segmentation [KQ04] [CC07]), the proposed segmentation system must be able to cope with a wide variety of structure shapes and image modalities. As automatic segmentations relying on the statistics of image intensities, mean organ shape or position do not work effectively for our purpose, we develop an efficient semi-automatic segmentation system. Fig. 1 shows the major components involved in our segmentation framework. Our approach combines image processing techniques and mathematical morphology operations to identify the tissue of interest and obtain an initial segmentation close to the target structure shape. The initial segmentation is then refined using a level set method, instead of growing a new segmentation from seed points as in previous approaches. For many cases, this framework requires little pre-processing on its input. Smoothing the input image is not usually required to produce reasonable solutions, though it may still be warranted in some cases.

Although this is a semi-automatic system, the required external interventions are limited to two interactive operations:

- Definition of a range of intensity values that classify the tissue type of interest, which is an alternative to automatic estimation based on intensity distribution;
- A seed point is placed in a desired region as an input to a simple region growing algorithm to provide the initialization for the level set approach. This can greatly reduce the labour requirement of manual seed placement used by other level set based approaches.

Unlike other level set based approaches, our system is not sensitive to the parameter settings. Default parameters are applied without the need to tune on a case by case basis. Furthermore, no information on general shape, location and orientation of an anatomical structure of interest is required in our system.

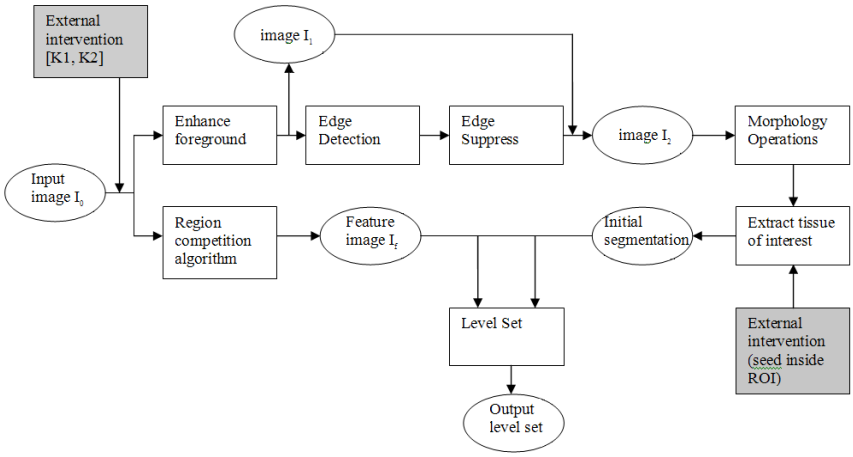

Fig. 1. Work flow

2 Methodology

A large body of work has explored the level set method and its applications in image segmentation [DMR*01] [WKW02]. Although the level-set technique is relatively insensitive to initial conditions, a reasonable prior segmentation as the initialization could 1) increase the chances of segmenting a complex object without missing parts and 2) help to reduce the amount of time needed by the front to propagate through a whole object and hence reduce the risk of leaks on the edges of regions visited earlier. Many approaches place seeds and implement a fast marching algorithm to grow the seeds as the initial segmentation which is the input of level set method applied afterward. The disadvantage is the initial segmentation result is sensitive to the seed positions and seed numbers. For example, when segmenting an elongated object, it is undesirable to place a single seed at one extreme of the object since the front will need a long time to propagate to the other end of the object. Obviously placing several seeds along the axis of the object is probably the best strategy to ensure that the entire object is captured early in the expansion of the front. However, this normally requires users with sufficient anatomical knowledge and it is also a non trivial process.

To overcome those shortcomings, we propose an initialization method which employs edge enhancement following by mathematical morphology operations to ensure that the major object structures could be captured. This prior segmentation will then be embedded into the level set function

for further refinement. As the level set then starts from a close approximation to the actual structure shape, this approach can improve the accuracy of results and dramatically decrease processing time. Consequently, the risk of leaks which is common to previous level set based approaches can be minimized.

In this section, our approach is demonstrated using an example of aorta segmentation. The abdominal CT data set was collected at an in-plane resolution of 0.84375mm by 0.84375mm with an inter-slice distance of 1mm. The data dimensions are 512×512 ×401. No contrast was infused. The images show slices through the point (284,271,203).

2.1 Segmentation Initialization

2.1.1 Edge enhancement

Generally speaking, the first step in automatic segmentation is region of interest (ROI) detection. A common approach is based on statistical estimation of image intensity values that could classify the tissue type of interest. Normally an assumption is made based on the intensity histogram of the ROI [RBN*07]. Sometimes the anatomical structures have to be used as guidance. For example, the liver is the biggest organ in the abdomen and adjacent to the lung area which always appears as the darkest region. Obviously, when the original images vary greatly in resolution and quality, and organ segmentation is not limited to liver, relying on such estimations is not sufficient. Alternatively, we provide interactive tools to explicitly define an interval $[K_1, K_2]$, where the intensity values of the tissue of interest lie. The same intensity interval $[K_1, K_2]$ is applied to calculate the feature image in section 2.2. Given an intensity range $[K_1, K_2]$, we have

$$I_1(x) = \begin{cases} I_0(x) & if \quad I_0(x) \in [K_1, K_2] \\ 0 & else \end{cases} \qquad (1)$$

The gradient magnitude of image I_1 at each pixel is computed (fig. 2b) and a lower hysteresis threshold T is applied to the result to suppress spurious edges, similar to that used in the Canny edge detection algorithm, as shown in fig. 2c. Currently, the threshold T is estimated using the histogram of the gradient image. However, an interactive way to adapt the threshold value in real time is also provided. The remaining edges are enhanced to the maximum intensity value $\boldsymbol{C}$ of image I_1. These can be briefly described as Equation 2:

$$I_1'(x) = \begin{cases} C & if \quad \nabla I_1(x) > T \\ 0 & else \end{cases} \qquad (2)$$

Next, image I_1' is subtracted from the image I_1. The resulting image I_2 is shown in fig. 2d. The image I_2 results in better performance than image I_1 when applying morphological operations to separate adjoining tissues, as discussed in the following section. Fig. 3 illustrates the differences.

$$I_2(x) = I_1(x) - I_1'(x) \qquad (3)$$

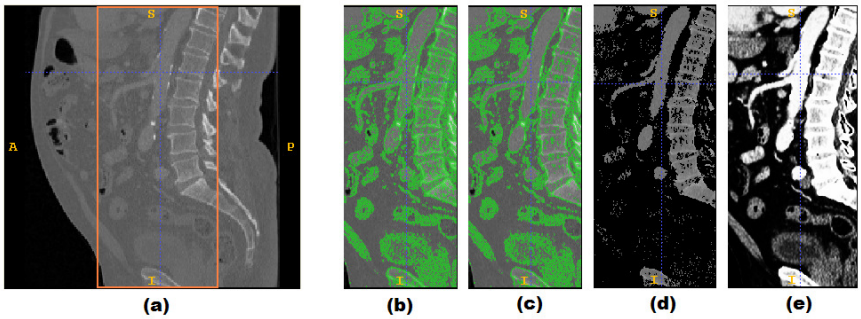

Fig. 2. Edge enhancement. (a) Original slice in sagittal view (image I_1). The area inside the rectangular box indicates the location of the abdominal aorta. (b) The gradient magnitude of image I_1 (only partial image I_1, i.e. the area inside the rectangular box of (a) is displayed). (c) Spurious edge suppression. (d) Image I_2 after subtracting the enhanced edge from image I_1 (e) Feature map of image I_0

2.1.2 Mathematical morphology scheme

We apply morphological erosion followed by interactive region growing algorithm to remove the areas that do not belong to the target organ. The morphological erosion is defined as:

$$E(I_2, B) = I_2 \Theta(-B) = \bigcap_{\beta \in B} (I_2 - \beta) \qquad (4)$$

B is the structure element, having: $-B = \{-\beta \mid \beta \in B\}$. By applying it to the image I_2, we can separate the adjoining tissues (as shown in fig. 3).

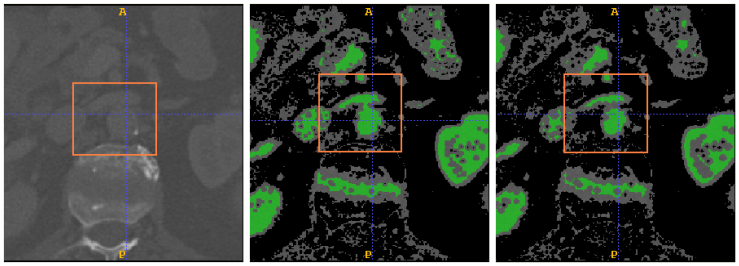

Fig. 3. Applying morphological erosion on images with or without edge enhancement. (a) Original slice in axial view (the square indicates the location of abdominal aorta). (b) Result without edge enhancement. (c) Result with edge enhancement, where the adjoining tissues have been correctly separated (indicated by the green color areas).

Next, the object regions are extracted to provide an initial segmentation to be embedded into the level set function. Although it may be possible to automatically identify the target organ from a set of candidate regions using prior knowledge of organ shape, for best efficiency and accuracy we simply provide a user interface to guide the extraction. Starting from a user-supplied seed point or a seed region, the system implements a simplified region growing algorithm based on connected-components to extract the target organ, as shown in fig. 4.

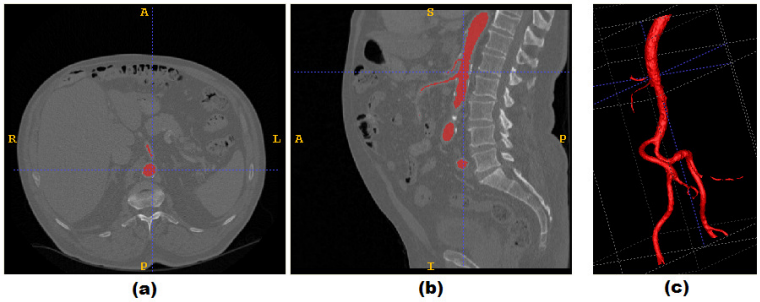

Fig. 4. Prior segmentation which is extracted from a set of candidate regions by placing one seed inside the region representing the real abdominal aorta. Red indicates the region of the prior segmentation. (a) original image in axial view. (b) original image in sagittal view. (c) 3D view of the prior segmentation result.

The initial segmentation is further refined by a level set approach. Using the property of keeping the evolution front smooth, this can reduce some of the "leaking" that is common in connected-component schemes, e.g. applications using region growing or morphology operations.

2.2 Level Set Initialisation

It is shown in section 2.1.2 that the initial segmentation is a good approximation of the actual organ shape. In this section, the accurate shape recovery is implemented in a modified form of the basic level set equation developed in [MSV95], i.e.

$$\frac{d}{dt}\psi + \alpha P|\nabla\psi| - \beta K|\nabla\psi| = 0 \qquad (5)$$

$\boldsymbol{\Psi}(x, t)$ is the level set function. The evolution front is obtained by extracting the zero level set i.e. $\boldsymbol{\Psi}(x, t)=0$. We embed the initial segmentation as an initial front of the function $\boldsymbol{\psi}$ at $t=0$. The propagation term P from Equation 5 is an image based force defined from the feature image $g(I)$. In our framework, we compute the feature image using a modified version of the region competition method by Zhu and Yuille [ZY96], where the intensity values fall in the interval [-1, 1]. Fig. 2e displays the feature image, which is calculated according to Equation 6. The intensities of the feature image have been mapped into the interval [0, 255].

$$g(I) = \{P_{obj}(i) - P_{back}(i) \quad i \in I\} \tag{6}$$

where $P_{obj}(i)$ is the probability that a pixel in the image belongs to the foreground; $P_{back}(i)$ is the probability that the pixel belongs to the background. The intensity ranges of the foreground and background have been defined in the section 2.1.1 in an interactive way.

2.3 Level Set Evolution

Fig. 5 shows some screen shots obtained at intermediate evolutions to demonstrate the idea that our approach requires less iterations and can efficiently reduce the risk of leaking at weak boundaries. For comparison, we also segmented the same dataset using SNAP[2] where its evolution speed is calculated based on the same feature map as ours (fig. 2e). As with other level set based applications, SNAP is sensitive to both the seed positions and seed numbers. Here, 27 seeds have been placed evenly along the aorta carefully avoiding areas close to weak edges (fig. 5d). Other parameters required by SNAP were set to the same values as ours if possible. For our approach, the segmentation is nearly complete at 60 iterations. At 115 iterations, the result has not changed significantly, nor have any "leaks" occurred in the result. In contrast, using SNAP the aorta shape has only been roughly formed at 240 iterations, except the left common iliac (fig. 5g). At 520 iterations, the aorta segmentation is completed. However, "leaking" has occurred between the abdominal aorta and the spine, as shown in fig. 5h.

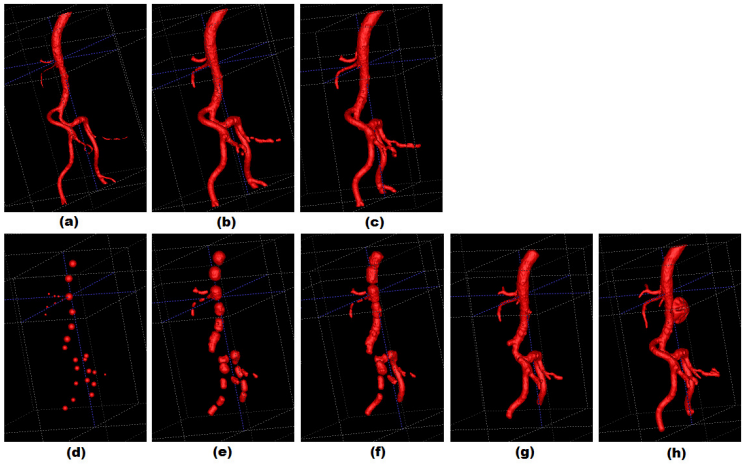

Fig. 5. Intermediate evolution results: comparison between our approach and SNAP. (a)-(c) our approach, showing results of (a) initial segmentation (b) at 60 iterations (c) at 115 iterations. (d)-(h) intermediate results from SNAP (d) initial segmentation by placing 27 seeds evenly along the aorta (e) at 60 iterations (f) at 115 iterations (g) at 240 iterations (h) at 520 iterations.

3. Evaluation and Experimental Results

3.1 Example results

Besides the aorta segmentation demonstrated in section 2, we visualize other segmentation results to illustrate that our method is a general approach for abdominal structure segmentation on varied image modalities. The same procedure and default parameters (as in section 2) were applied to obtain aorta, vein, kidney and liver segmentations (fig. 6). Fig. 6a shows a result from a high resolution CTA image provided by St. Mary's London Hospital & Imperial College London. The result in Fig. 6b is also from contrast enhanced CT, but at low resolution (provided by St James's University Hospital Leeds). Fig. 6c shows the segmentation from a CT image provided by Royal Liverpool University Hospital with no contrast infused. This is a typical case of right renal obstruction used in a VE for performing nephrostomy. Fig. 6d is from an MR renal donor angiogram image with contrast infused, provided by Royal Liverpool University Hospital, which is used to construct a VE of renal collecting system.

[2] SNAP is an application developed on the National Library of Medicine Insight Segmentation and Registration Toolkit (ITK). http://www.itksnap.org or as part of ITK from http://www.itk.org

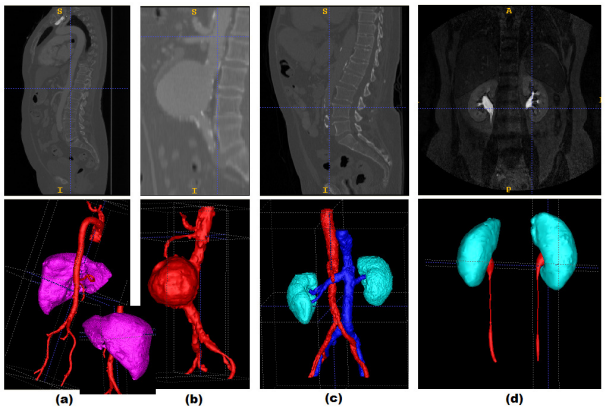

Fig. 6. Abdominal structure segmentations. (a) 275th slice (sagittal view) in image of dimension 512×512×615. (b) 117th slice (sagittal view) in image of dimension 230×200×346. (c) 284th slice (sagittal view) in image of dimension 512×512×423. (d) 39th slice (coronal view) in image of dimension 384×384×65.

The successful segmentation demonstrates the wide applicability of the work. Current tests demonstrate that other image modalities such as CT, MR and Angiogram images etc. could be suitable to segment abdominal structures and create the virtual environments. The approach is however unlikely to be successful for modalities with very poor SNR such as Ultrasound. As CT images are our major resource for creating virtual human anatomy, the evaluations in the following section focus on CTA image segmentation.

3.2 Evaluation of accuracy

We evaluated our method on 17 cases where the manual segmentation results were provided by Imperial College London. All cases are contrast enhanced images (CTA) of high resolution (provided by St. Mary's London Hospital). The segmentation results include ascending aorta, arch of the aorta, brachiocephalic arteries, common carotids, subclavian arteries, descending aorta, celiac artery, superior mesenteric artery, renal artery, common iliac arteries, external lilac arteries, internal iliac arteries and common femoral arteries. Table 1 lists some representative comparison results. The numeric evaluation is based on the measurement of volume overlapping rate [ULS*02] and voxel distance. Manual segmentation results are taken as reference models.

Table 1. Evaluation results.

Dataset	FNVF	FPVF	TPVF	Max. Positive Dist. [mm]	Max. Negative Dist. [mm]	Ave. Positive Dist. [mm]	Ave. Negative Dist. [mm]
STM002	0.1764	0.1329	0.8236	35.15	25.48	2.91	2.31
STM003	0.1016	0.0286	0.8984	32.81	21.09	2.72	2.07
STM004	0.1083	0.0706	0.8917	20.26	10.91	2.56	2.04
STM005	0.1575	0.0389	0.8425	26.62	12.85	2.79	2.40
STM006	0.1636	0.0824	0.8364	27.25	17.03	2.58	2.37
STM007	0.1511	0.0789	0.8489	31.38	23.77	3.11	2.35
STM008	0.1368	0.0567	0.8632	36.70	24.75	3.02	2.28
STM009	0.1371	0.0367	0.8629	30.69	12.27	2.43	2.69
STM010	0.2469	0.0638	0.7530	28.94	26.66	2.33	2.30
STM011	0.0814	0.0577	0.9186	16.60	16.60	2.57	2.87
STM012	0.0552	0.1246	0.9448	20.39	21.28	2.47	2.45
STM013	0.0843	0.0732	0.9157	40.62	14.06	2.24	2.08

FNVF: False Negative Volume Fraction	Max. Positive Dist.: The maximum distance when reference model is the result of our method.
FPVF: False Positive Volume Fraction	Max. Negative Dist.: The maximum distance when the reference model is manual segmentation.
TPVF: True Positive Volume Fraction	Standard Positive Dev.: The standard deviation of Max. Positive Dist.
	Standard Negative Dev.: The standard deviation of Max. negative Dist.

TPVF denotes the fraction of the total amount of tissue in reference model with which our result overlaps. The relatively low volume overlap rate is caused by the inconsistent segmentation along the aorta medial axis when it is performed by different observers. The main differences between our result and the manual segmentation are at the common carotids, subclavian arteries and renal artery (as shown in fig. 7c). Although there is a basic segmentation guidance on which part of the aorta should be segmented, it is impossible to define case by case on how far those branches should be presented in the segmentation result. Fig. 7 visualizes the differences using the case of STM002, where the blue depicts those voxels which are missed by our method but included by the manual segmentation (mainly at

common carotids, subclavian arteries and ascending aorta); the yellow illustrates voxels which are missed by the manual segmentation but correctly identified by our method (mainly at the renal artery and external iliac arteries). Here, red indicates voxels of being segmented by both methods. When results are evaluated explicitly on the specified areas which are common to both methods, the performance improves significantly, as shown in Table 2. The datasets STM002 and STM010 are taken as examples, as they currently have the worst performances.

Table 2. Performance evaluation is carried out explicitly on the specified areas

Dataset	FNVF	FPVF	TPVF
STM002	0.0434	0.1002	0.9566
STM010	0.0551	0.0414	0.9449

The segmentation resolution can also cause differences between two methods. This can be seen in fig. 7, where the descending aorta has been amplified and displayed at the right corner of (a) and (b), respectively. As shown in fig. 7a, being done slice by slice on DICOM data, the manual segmentation normally has aliasing artefacts in the result. On the contrary, our method refines the segmentation using the level set, which helps to smooth the blood vessel wall, as shown in fig. 7b.

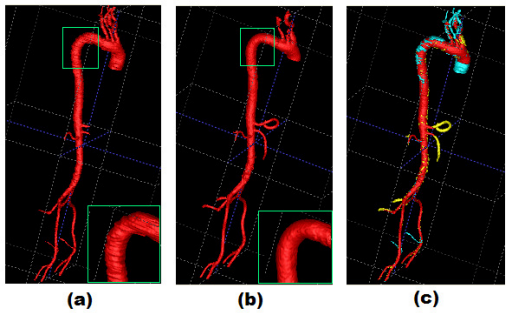

Fig. 7. Visualization of the differences between our result and the manual segmentation result on case STM002. (a) Manual segmentation result. (b) Our segmentation result. (c) Visualization of differences.

3.3 Evaluation of efficiency

The practical viability should also be considered when evaluating a semi-automatic segmentation method. The computational time and the human operator time required to complete segmentation can be used to characterize the efficiency of a segmentation method.

Our system includes computing the image gradient and the level set task for which the computational time increases significantly when image resolution and data size increases. The datasets in table 1 have also been used to test the efficiency of our system. From the data we currently have, they represent the largest volume size and the highest resolution. The data resolutions range from 0.779297mm×0.779297mm×1mm to 0.951172mm×0.951172mm×1mm. The data dimensions vary from 512×512×554 to 512×512×659. All 17 cases are contrast-enhanced CTA. Because of the simplicity of the user interactions in our system, the human operation time is negligible compared to the computational time of the image processing and level set tasks, so we do not time them separately. The evaluation is carried on a PC with a Core2 CPU at 2.66GHz. The average segmentation time is 5 minutes to obtain the segmentation accuracy shown in table 1. In contrast, for another semi-automatic level set based approach (SNAP), a minimum of 2 hours is needed for the same dataset, where the segmentations were completed by an experienced medical student. No exact operation time has been given for the manual segmentation.

4 Conclusion and Future Work

One of our primary motivations in developing this framework is to achieve both greater efficiency and accuracy in segmentation on a variety of image modalities and for a variety of structures. Our approach combines image processing techniques and mathematical morphology operations to identify the tissue of interest and obtain an initial segmentation close to the target structure shape. The initial segmentation is automatically embedded into the level set function to obtain a refined segmentation result. Note that only minor intervention is required to set up individual computations. Traditional seed

positioning is replaced by seed fronts representing a good approximation to the original structures. Consequently only 50 to 70 iterations are needed to propagate to the structure boundaries. This dramatically decreases processing time and reduces the risks of leaking at the weak boundaries, without compromising the accuracy of segmentation. Currently, the default parameters used by our system work well in a variety of image modalities, such that adjustment of these parameters for each case which is common in other level set based methods tends not to be necessary. The evaluation will be extended to other image modalities as manual segmentations become available.

Acknowledgements:

This work is funded by the UK Engineering & Physical Science Research Council (EP/E002749). The authors would like to thank Dr Fernando Bello and Dr Vincent Luboz from Imperial College (St. Mary's London Hospital) for help with collecting the test data and providing manual segmentations for evaluations. We would also like to thank Dr Derek Gould in University of Liverpool for data acquisition and valuable clinical advice.

References

[CC07] Campadelli, P. and Casiraghi, E. (2007) Liver Segmentation from CT Scans: A Survey. Lecture Notes in Computer Science, Springer Berlin, vol. 4578, pp. 520-528, August.

[CKS97] Caselles, V., Kimmel, R. and Sapiro, G. (1997) Geodesic Active Contours. International Journal of Computer Vision, 22(1) 6179.

[DMR*01] Droske, M., Meyer, B., Rumpf, M. and Schaller, K. (2001) An adaptive Level Set Method for Medical Image Segmentation. Presented in 17th International Conference on Information Processing in Medical Imaging.

[GHF98] Gao, L., Heath, D.G., Fishman, E.K. (1998) Abdominal Image Segmentation Using Three-dimensional Deformable Models. Investigative Radiology 33(6), pp. 348-355.

[HMW07] Heimann, T., Meinzer, H.P. and Wolf, I. (2007) A Statistical Deformable Model for the Segmentation of Liver CT Volumes. MICCIA 2007 workshop proceedings.

[KQ04] Kirbas, C. and Quek, F. (2004) A Review of Vessel Extraction Techniques and Algorithms. ACM Computing Surveys, vol. 36, no. 2, pp. 81-121, June.

[MBW*05] Museth, K., Breen, D.E., Whitaker, R.T., Mauch, S., and Johnson, D. (2005) Algorithms for Interactive Editing of Level Set Models. Computer Graphics Forum 24, 4, 1--22.

[MSV95] Malladi, R., Sethian, J.A. and Vemuri, B.C. (1995) Shape Modeling with Front Propagation: A Level Set Approach. IEEE Trans. Pattern Analysis and Machine Intelligence, vol. 17, No. 2, September.

[PBM03] Park, H., Bland, P.H. and Meyer, C.R. (2003) Construction of an Abdominal Probabilistic Atlas and Its Application in Segmentation. IEEE Transactions on Medical Imaging, vol. 22, no. 4, pp. 483-492, April.

[PD01] Pan, S. and Dawant, B.M. (2001) Automatic 3D Segmentation of the Liver from Abdominal CT images: A Level-set Approach. Proc. SPIE-Int. Soc. Opt. Eng., Medical Imaging 2001: Image Processing, San Diego, CA, Feb. pp. 19-22.

[PT01] Pohle, R., Toennies, K.D. (2001) Segmentation of Medical Images Using Adaptive Region Growing. Proc. SPIE Medical Imaging 4322, pp. 1337-1346.

[RBN*07] Rusko, L., Bekes, G., Nemeth, G. and Fidrich, M. (2007) Fully Automatic Liver Segmentation for Contrast-enhanced CT Images. MICCIA 2007 workshop proceedings.

[Set99] Sethian, J.A. (1999) Level Set Methods and Fast Marching Methods: Evolving Interfaces in Computational Geometry, Fluid Mechanics, Computer vision, and Material Science. Cambridge University Press, UK.

[SLR*02] Suri, J.S., Liu, K., Reden, L. and Laxminarayan, S. (2002) A Review on MR Vascular Image Processing: Skeleton Versus Nonskeleton Approaches II. IEEE Trans. on Information Technology in Biomedicine, vol. 6, no. 4, December.

[ULS*02] Udupa, J., LeBlanc, V., Schmidt, H., Imielinska, C., Saha, P., Grevera, G., Zhuge, Y., Molholt, P., Jin, Y. and Currie, L. (2002) A Methodology for Evaluating Image Segmentation Algorithm. SPIE Conf. on Medical Imaging, San Diego CA, USA.

[WBM*01] Whitaker, R.T., Breen, D.E., Museth, K. and Soni, N. (2001) A Framework for Level Set Segmentation of Volume Datasets. Volume Graphics 2001 Proceedings, pp 159-68.

[WKW02] Watanabe, M., Kikinis, R. and Westin, C. (2002) Level Set Based Integration of Segmentation and Computational Fluid Dynamics for Flow Correction in Phase Contrast Angiography. Lecture Notes in Computer Science, vol. 2489. Proc. 5th Int. Conf. on MICCAI, pp. 405 – 412.

[WTH*98] Wang, K.C., Taylor, C.A., Hsiau, Z., Parker, D. and Dutton, R.W. (1998) Level Set Methods and MR Image Segmentation for Geometric Modelling in Computational Hemodynamics. Proc. 20th Annual International Conference of the IEEE Engineering in Medicine and Biology Society, vol. 20, no. 6.

[YCN*00] Too, S.W., Cho, J.S., Noh, S.M., Shin, K.S. and Park, J.W. (2000) Organ Segmentation by Comparing of Grey Value Portion on Abdomial CT image. Proc. 5th Int. Conf. on Signal Processing, Beijing, pp. 21-25.

[ZY96] Zhu, S.C. and Yuille, A. (1996) Region Competition: Unifying Snakes, Region Growing, and Bayes/MDL for Multiband Image Segmentation. IEEE Trans. on Pattern Analysis and Machine Intelligence, vol. 18, No. 9, September.